Electrodeposition and dissolution of Co–W alloy films

C.L. ARAVINDA[1], V.S. MURALIDHARAN[2] and S.M. MAYANNA[1]*
[1]*Department of Postgraduate Studies in Chemistry, Central College, Bangalore University, Bangalore 560 001, India*
[2]*Central Electrochemical Research Institute, Karaikudi, 630 006, India*
(*author for correspondence)

Abstract

Cyclic voltammetric studies were carried out on platinum in alkaline solution containing cobalt sulphate, sodium tungstate, dimethyl sulphoxide and triammonium citrate. Spectral u.v. absorption studies of cobalt citrate complex indicate the species to be $[Co\ L\ (H_2O)_3]^{2+}$, where L is triammonium citrate. The deposition of cobalt involves a stepwise electron transfer mechanism. The observed cyclic voltammetric data show that the alloy deposition is possibly from cobalt–tungstate complex. The citrate ions and dimethyl sulphoxide hinder the alloy deposition. Dimethyl sulphoxide, which specifically adsorbs on the electrode surface, favours the hydrogen evolution reaction (HER), whereas tungstate hinders the HER. Stripping voltammograms show the existence of cobalt rich alloy phases. X-ray diffraction studies further confirm the phases to be Co_3W and Co_7W.

1. Introduction

Tungsten forms hard alloys with iron group metals especially with cobalt and nickel, retaining some of its unusual magnetic, electrochemical and mechanical properties, even at elevated temperature, and also exhibiting good corrosion resistance towards acidic and alkaline media [1–5]. In recent years several methods have been used to deposit tungsten alloys of which electroplating is gaining importance. The early review of Still and Dennis [6] on the subject is noteworthy. Alloys of tungsten free from surface contaminants [7] and exhibiting good functional properties [8, 9] were electroplated from complex bath solutions.

Alloy plating is a complex process as the functional properties of the alloys depend on the bath composition and plating conditions [10, 11]. The understanding of the electrochemical reduction of tungstate in the presence of iron group metals is still in its infancy [12]. Voltammetric behaviour of Co^{2+} and WO_4^{2-} ions in the plating bath solution during the electrodeposition of Co–W alloy has been studied [13]. The present communication reports a cyclic voltammetric study of the role of dimethyl sulphoxide (DMSO) and triammonium citrate (TAC) during electroplating of Co–W alloys.

2. Experimental details

All solutions were prepared using double distilled water and AR grade chemicals. $CoSO_4$, 0.02 M; Na_2WO_4, 0.02 M solutions containing triammonium citrate (TAC) $\{0.01\,M < x < 0.1\,M\}$ or dimethyl sulphoxide (DMSO) $\{0.01\,M < x < 0.1\,M\}$ or both were used along with Na_2SO_4 0.01 M and boric acid 0.05 M. The pH of the medium was maintained at 8.0 by adding sodium hydroxide solution and using a digital pH meter. Experiments were conducted at 298 K.

Voltammetric experiments were carried out in a single compartment cell. A miniature platinum electrode and a large platinum foil were used as working and counter electrodes respectively. The potentials of the working electrode were monitored by using a scanning potentiostat (EG&G, PAR model 362). The voltammograms were recorded only after obtaining reproducible responses on repeated scanning. Ultraviolet absorption spectra of the solutions were recorded using spectrometer [Hitachi 150–20, Japan]. An X-ray diffractometer [Philips, PW 1140/90] was used to characterize the phases of the alloy deposit and of the heat-treated (under N_2 atmosphere at 400 °C for 4 h) plated foils.

3. Results

3.1. *Influence of supporting electrolytes*

Figure 1 represents the typical cyclic voltammograms obtained in TAC solution of different concentrations. When polarized from 0 to −1100 mV, the forward scan exhibits no cathodic peak and hydrogen evolution occurs beyond −900 mV. The reverse scan exhibits an
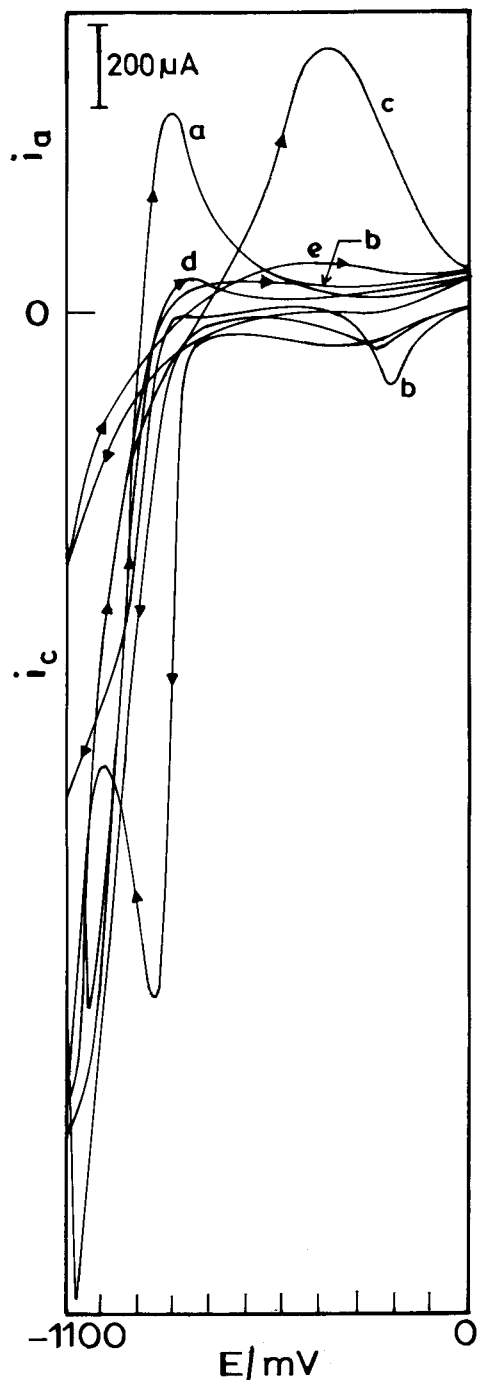
Fig. 1. Cyclic voltammograms obtained in various solutions (with Na$_2$SO$_4$ 0.01 M, boric acid 0.05 M, at pH 8, $v = 25$ mV s^{-1}): (a) TAC 0.05 M; (b) DMSO 0.05 M; (c) TAC 0.05 M + CoSO$_4$ 0.02 M; (d) DMSO 0.05 M + Na$_2$WO$_4$ 0.02 M; (e) TAC 0.05 M + Na$_2$WO$_4$ 0.02 M.

anodic peak at -698 mV, which may be due to the oxidation of absorbed hydrogen or partial oxidation of citrate ions (Figure 1(a)). Introduction of DMSO into the solution gives a cathodic peak at -186 mV. Anodic peaks are not seen in the reverse scan (Figure 1(b)). Introduction of Co^{2+} ions in to the solution results in the appearance of a cathodic peak at -922 mV followed by hydrogen evolution beyond -1000 mV. The reverse scan exhibits a broad anodic peak around -313 mV (Figure 1(c)), suggesting the anodic dissolution of

cobalt. Sodium tungstate solution does not show a peak in either scan (Figure 1(e)). However, in the presence of DMSO, a small hump appears around -450 mV in the forward scan which is followed by hydrogen evolution (Figure 1(d)). This suggests that the tungstate ion undergoes reduction in the presence of DMSO. The reverse scan exhibits a broad peak around -800 mV, suggesting the dissolution of tungsten.

3.2. Influence of TAC

Figure 2 represents the cyclic voltammograms obtained in the solution containing Co^{2+} ions and TAC. While scanning the potentials from 0 to -1100 mV, a distinct cathodic peak appears at -83 mV, which becomes more negative with sweep rate (Figure 2). Hydrogen evolution (HER) occurs beyond -700 mV. The reverse scan exhibits a broad anodic peak around -423 mV, which becomes more positive with sweep rate. An increase in TAC concentration exhibits interesting features. In 0.01 M solution, a reduction peak (Figure 3(a)) appears at -950 mV followed by hydrogen evolution. In 0.05 M solution, a cathodic peak (Figure 3(b)) appears at -83 mV, which predominates with increase in the concentration of TAC (Figure 3(c)). In the reverse scan a small hump around -700 mV followed by a sharp peak at -450 mV appears in 0.1 M TAC solution. This suggests stepwise dissolution of Co^{2+} ions and the monovalent species being stabilized by citrate ions.

3.3. Influence of sodium tungstate

The presence of sodium tungstate markedly changes the voltammogram characteristics. During the forward scan, a shoulder appears around -900 mV, which
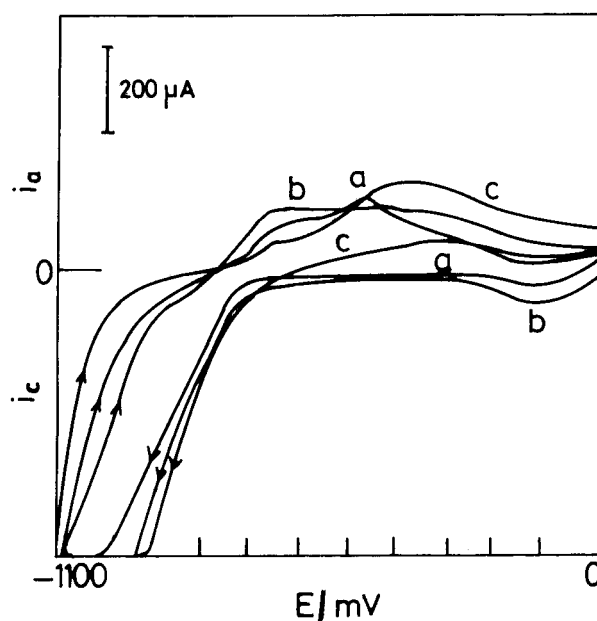

Fig. 2. Cyclic voltammograms obtained in solution of CoSO$_4$ 0.02 M + TAC 0.05 M (with Na$_2$SO$_4$ 0.01 M, boric acid 0.05 M at pH 8 at different scan rates: (a) 25, (b) 50 and (c) 100 mV s^{-1}.
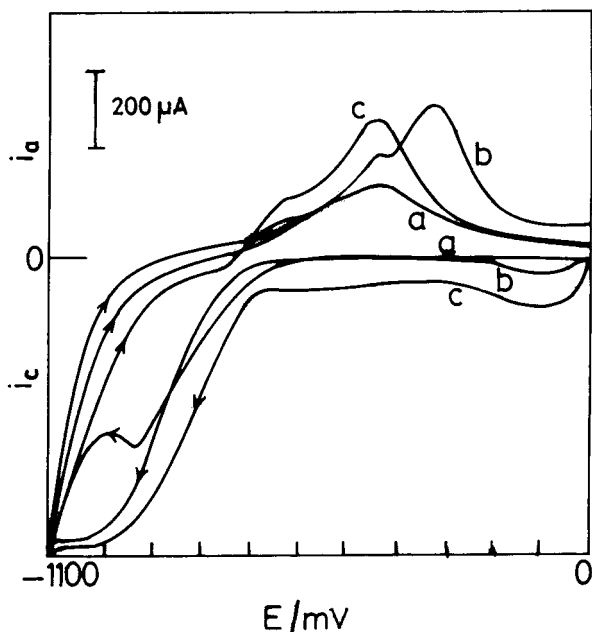
Fig. 3. Cyclic voltammograms obtained in $CoSO_4$ 0.02 M and solutions (with Na_2SO_4 0.01 M, boric acid 0.05 M, pH 8, $v = 25$ mV s^{-1}) containing different concentrations of TAC: (a) 0.01, (b) 0.05 and (c) 0.1 M.

become predominant with an increase in WO_4^{2-} ion concentration. The reverse scan exhibits a distinct anodic peak at -462 mV (Figure 4(a)). An increase in WO_4^{2-} ion concentration by four folds shows an additional anodic peak (Figure 4(b)), suggesting the dissolved species being stabilized by WO_4^{2-} ions.

3.4. Influence of DMSO

Figure 5 represents the cyclic voltammograms obtained in the solution containing $CoSO_4$, Na_2WO_4 and DMSO. During the potential scan from 0 to -1100 mV, the forward scan exhibits a shoulder (Figure 5(b)) around -950 mV, which becomes a plateau with rise in DMSO concentration (Figure 5(a)). The anodic peak splitting disappears at lower concentration, and a single anodic peak (Figure 5(c)) appears at 0.01 M DMSO with a shift to more negative potential suggesting that DMSO hinders the dissolution of the Co–W alloy.

3.5. Effect of sweep rate

Figure 6 represents the electrochemical spectrum obtained in the presence of all the species in plating bath solution. The forward scan exhibits a small cathodic hump around -950 mV, which disappears at higher sweep rate. The reverse scan exhibits a broad anodic peak around -400 mV, which becomes sharper with increase in sweep rate.

4. Discussion

The u.v. absorption spectrum (Figure 7) of an aqueous solution containing Co^{2+} ions and TAC shows a sharp
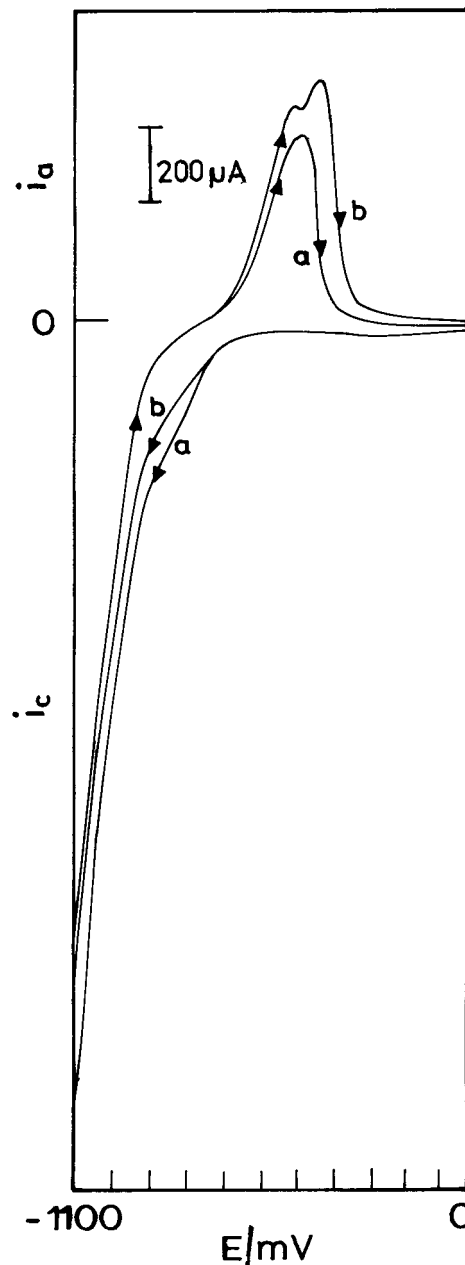

Fig. 4. Cyclic voltammograms obtained in solution (with Na_2SO_4 0.01 M, boric acid 0.05 M at pH 8, $v = 25$ mV s^{-1}) $CoSO_4$ 0.02 M + TAC 0.05 M + DMSO 0.05 M containing different concentrations of Na_2WO_4: (a) 0.01 and (b) 0.04 M.

peak at 532 nm and a broad hump around 717 nm. Based on these data, the assigned transitions are $^4T_1g \rightarrow {}^4T_1g$ (r$_2$) and $^4T_2g \rightarrow {}^2A_2g$ (r$_3$), respectively, for Co^{2+} ion in an octahedral arrangement leading to the complex with a structure $[Co\,L\,(H_2O)_3]^{2+}$, where L is the TAC. A similar spectral study with bath solution does not give positive results regarding the complexation of Co^{2+} ions with DMSO and sodium tungstate with DMSO or TAC.

4.1. Deposition of Co–W alloy

Many theories and mechanisms have been proposed for the deposition of reluctant metal like W in the presence
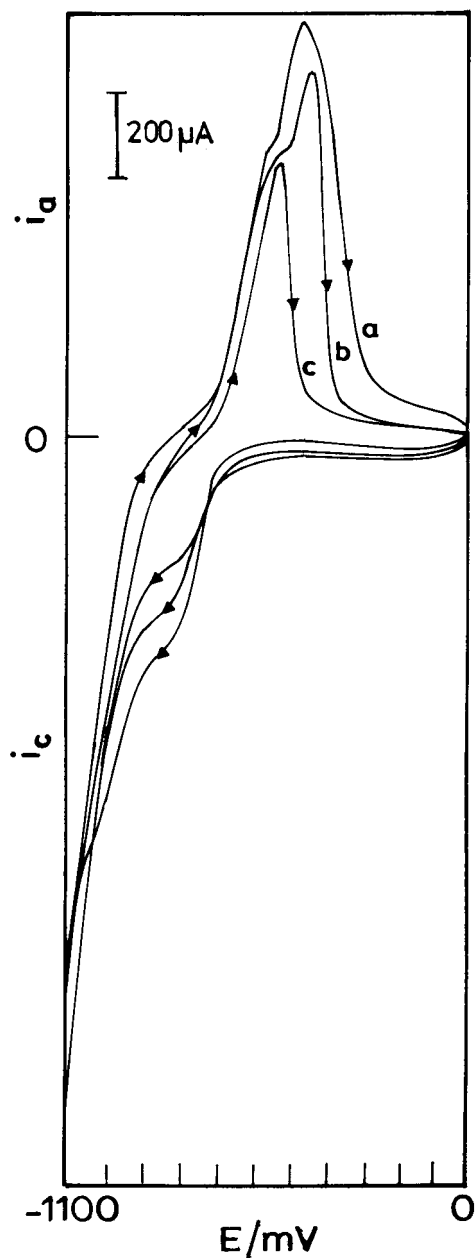
Fig. 5. Cyclic voltammograms obtained in solution (with Na_2SO_4 0.01 M, boric acid 0.05 M, at pH 8, $v = 25$ mV s^{-1}) $CoSO_4$ 0.02 M + Na_2WO_4 0.02 M + TAC 0.1 M containing different concentrations of DMSO: (a) 0.1, (b) 0.05 and (c) 0.01 M.
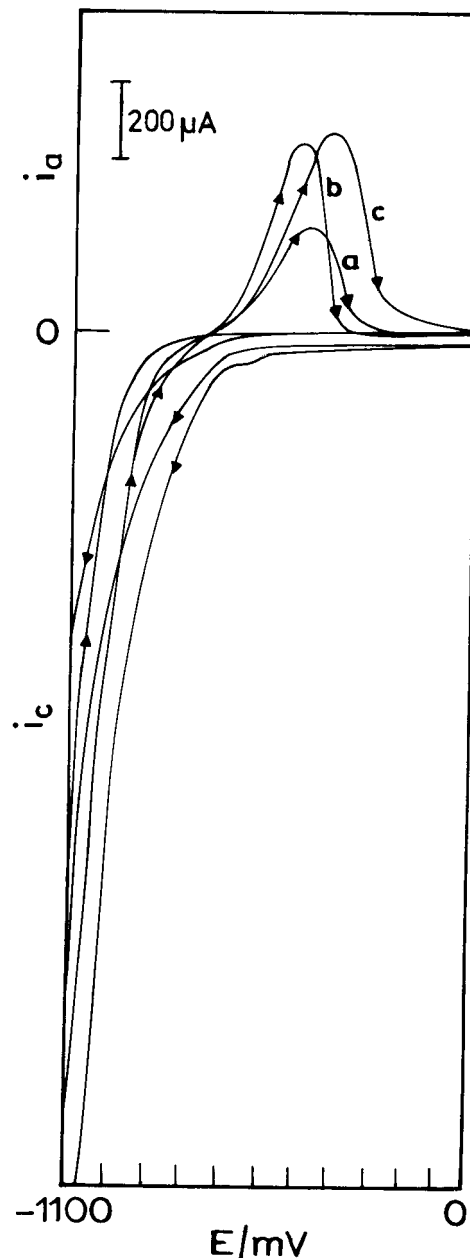
Fig. 6. Cyclic voltammograms obtained in solution of (with Na_2SO_4 0.01 M, boric acid 0.05 M, at pH 8) $CoSO_4$ 0.02 M + Na_2WO_4 0.02 M + DMSO 0.05 M + TAC 0.05 M, at different scan rates: (a) 10, (b) 25 and (c) 50 mV s^{-1}.

of iron group metals. However, some of these theories lack experimental evidence. In the present study, the appearance of a peak at −900 mV, which becomes predominant with an increase in WO_4^{2-} ion concentration, suggests the possibility of deposition of Co–W alloy from cobalt–tungstate complex. This is in accordance with earlier work [14]. The appearance of an anodic peak at −462 mV and its splitting at higher WO_4^{2-} ion concentration is suggestive of the dissolution of cobalt from a cobalt rich phase and the leaching of cobalt is facilitated by WO_4^{2-} ions. The cathodic peak current decreases with TAC concentration and $\{d \log I_{p,c}/d \log(TAC)\} = -1.5$ suggests that the TAC

preferentially complexes with Co^{2+} ions and prevents the discharge of Co^{2+} and WO_4^{2-} ions.

Co(II) complex undergoes reduction in succession as follows:

$$Co(\text{II}) \text{ complex} + e^- \rightarrow Co(\text{I}) \text{ complex} \qquad (1)$$

$$Co(\text{I}) \text{ complex} + e^- \rightarrow Co + \text{complex} \qquad (2)$$

Increase in TAC concentration favours the reduction of Co(II) complex and stabilizes the monovalent cobalt species. The cathodic peak currents are invariant with WO_4^{2-} ion concentration suggesting that the TAC
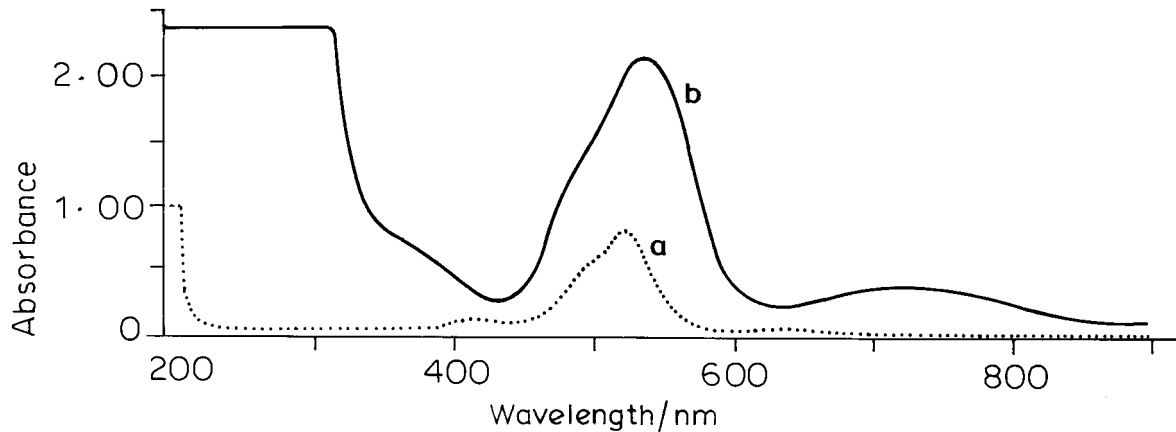
Fig. 7. Ultraviolet absorption spectra of solutions: (a) TAC 0.1 M and (b) CoSO$_4$ 0.02 M + TAC 0.1 M.

complexes with all Co^{2+} ions while only a fraction forms tungstate complex.

4.2. Hydrogen evolution reaction

The HER occurs only above −900 mV from alkaline citrate solutions containing WO$_4^{2-}$ ions. The electrodeposited alloy may offer higher hydrogen overvoltage. Figure 8 represents log I against E curves for the HER obtained at a sweep rate of 10 mV s^{-1} with different concentrations of tungstate. An increase in tungstate concentration accelerates the HER. Figure 9 represents log I against E curves for the her obtained at a definite sweep rate (10 mV s^{-1}) at different concentrations of DMSO. An increase in DMSO concentration also accelerates the her. The DMSO molecules may specifically adsorb on the surface of the cathode and stimulate the electrochemical discharge of water, as the sulphur compounds are known to act as effective reducing agents [15].
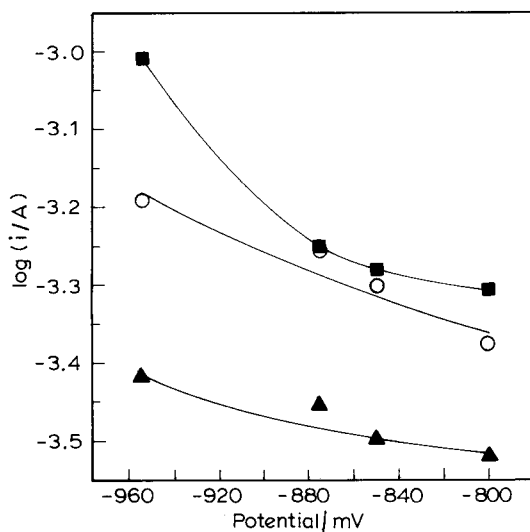
4.3. Dissolution of Co–W alloy films

The zero current crossing potentials (zccp's) observed during the reverse scan in the cyclic voltammograms are the corrosion potentials of the alloys in the medium. The corrosion potentials become nobler with increase in Co^{2+} ion concentration in solution and the anodic peak intersection potentials are invariant with Co^{2+} ions.

The reversible potential of W/WO$_4^{2-}$ ions in solution at pH 8 can be calculated:

$$W + 8\,OH^- \rightarrow WO_4^{2-} + 4\,H_2O + 6\,e^- \tag{3}$$
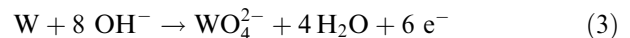
$$E_{r,W} = E_W^\circ + (RT/6F)\ln\{a_{WO_4^{2-}}\} \tag{4}$$

where E_W° is the standard potential for tungsten and $a_{WO_4^{2-}}$ is the activity of the tungsten ions.

$$E_{r,W-alloy} = E_W^\circ + (RT/6F)\ln\{a_{WO_4^{2-}}/a_{W-alloy}\} \tag{5}$$

$E_{r,alloy}$ is the reversible potential of tungsten in the intermetallic compound (it is assumed that the surface

Fig. 8. Log I against E curves for H$_2$ evolution reaction. Effect of tungstate concentration. Key: (▲) 0.005 M, (○) 0.01 M, (■) 0.02 M.
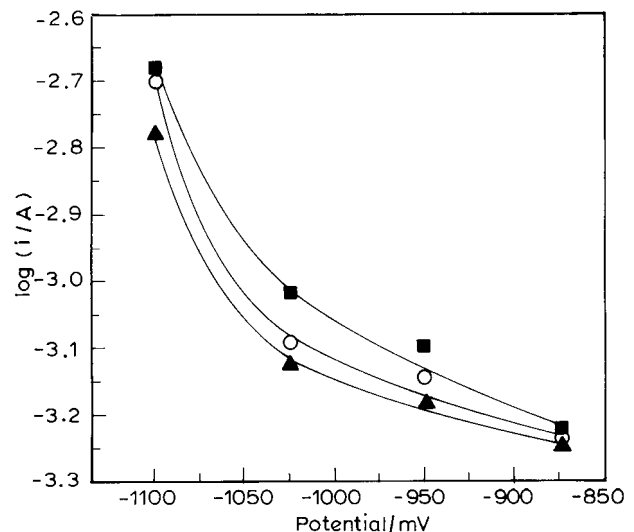

Fig. 9. Log I against E curves for H$_2$ evolution reaction. Effect of DMSO concentration. Key: (▲) 0.01 M, (○) 0.05 M, (■) 0.10 M.

Table 1. Parameters obtained from cyclic voltammograms

Solution composition molar ratio, Co:W	Zero current crossing potential (zccp) /mV	Anodic peak potential /mV	Anodic peak intersection potential /mV	ΔG, free energy change /kJ mol^{-1}
0:1	−628	−462	−560	−
1:1	−584	−457	−555	−1.34
4:1	−453	−453	−523	−10.37
10:1	−491	−457	−491	−18.49

$E_{\lambda,c} = -1100$ mV; $E_{\lambda,a} = 0$ mV; $v = 25$ mV s^{-1}. Solution composition/M: CoSO$_4$, 0.02; Na$_2$WO$_4$, 0.02; DMSO, 0.05; TAC, 0.05; Na$_2$SO$_4$, 0.01; H$_3$BO$_3$, 0.05, pH 8

Table 2. XRD data obtained* on Co–W codeposits

2θ	d/nm	Phase
As deposited		
47.78	2.2120	Co$_3$W (200)
58.96	1.8797	Co$_3$W (102)
89.08	1.2798	Co$_3$W (220)
After heat treatment		
47.77	2.2117	Co$_3$W (220)
51.36	2.0663	Co$_3$W (002)
54.52	1.9502	Co$_3$W (201)
70.26	1.5502	Co$_7$W (216)
88.76	1.2806	Co$_3$W (220)

*CuK_{α} radiation
Heat-treated at 400 °C for 4 h under N$_2$ atmosphere

energy contribution at the interface of alloy/electrolyte is negligible). $a_{W-alloy}$ is the activity of the tungsten in the intermetallic compound.

The difference (Equation 4− Equation 5) is thus:

$$-\Delta E = E_{r,W} - E_{r,W-alloy} = (RT/6F)\ln\{a_{W-alloy}\}$$
(6)

$$-6F\Delta E = RT\ln\{a_{W-alloy}\} = \Delta G$$
(7)

As a first approximation, $\Delta G = -6F\Delta E$. The free energy of alloy formation can be calculated [16] from the anodic peak intersection potentials for the W and Co–W alloy phases (Table 1). Variation of ΔG with increase in cobalt content indicates the formation of inter metallic phases rich in cobalt. Table 2 represents the X-ray diffraction data obtained on the alloy deposit on copper substrate before and after heat treatment. The deposits have hcp structure. On heat treatment, the additional new phases Co$_7$W (216) and Co$_3$W (002) are formed.

5. Conclusions

TAC preferentially complexes with Co^{2+} ions and prevents discharge of both Co^{2+} and WO$_4^{2-}$ ions. The discharge of Co^{2+} ions becomes appreciable at higher concentration of TAC. The mechanism of deposition of Co^{2+} ions occurs via a stepwise electron transfer reaction involving Co$^+$ ion as an intermediate. DMSO in the bath accelerates the deposition of tungsten and the evolution of hydrogen and retards the Co–W alloy dissolution process. Dissolution of cobalt from cobalt rich phase in the alloy occurs only at appreciable concentration of WO$_4^{2-}$ ions. The variation of free energy with cobalt content during alloy deposition indicates the existence of intermetallic phases rich in cobalt. New phases appear in the crystal lattice on heat treatment of the deposited alloy.

References

1. U. Admon and M.P. Dariel, *J. Appl. Phys.* **62** (1987) 1943.
2. J.P. Wittewaur and T.G. Nietu, *Ad. Mater. Process.* **142** (1992) 28.
3. F. Gartner, B. Junk and H. Kreye, *Galvanotechnik.* **90** (1999) 996.
4. J. Bhattarai, E. Akiyama, H. Habazaki, A. Kawashima, K. Asami and K. Hashimoto, *Corros. Sci.* **40** (1998) 155.
5. L. Ramesh, B.S. Sheshadri, and S.M. Mayanna, *Trans IMF* **76** (1998) 101.
6. F.A. Still and J.K. Dennis, *Electroplat. Met. Finish.* **26** (1974) 9.
7. S.M. Mayanna, L. Ramesh, B.N. Maruthi and D. Landolt, *J Mater. Sci. Lett.* **16** (1997) 1305.
8. L. Ramesh, B.S. Sheshadri and S.M. Mayanna, 'Royal Society of Chemistry' (Special publication: 'Chemistry, Energy and Environment') **217** (1998), p. 505.
9. B.N. Maruthi, L. Ramesh, S.M. Mayanna and D. Landolt, *Plat. Surf. Finish.* **86** (1999) 85.
10. S.M. Mayanna, N. Munichandraiah and T. Mimani, *J. Appl. Electrochem.* **23** (1993) 339.
11. S.M. Mayanna and T. Mimani, *Surf. Coat. Technol.* **79** (1996) 246.
12. T.A. Alekhina, I.A. Shoshina and B.G. Karbasov, *Electrokhimiya* **30** (1994) 285.
13. K. Wikiel and J. Osteryoung, *J. Appl. Electrochem.* **22** (1992) 506.
14. A.J. Bard (Ed.), 'Encyclopedia of Electrochemistry of the Elements', Vol. 5 (Marcel Dekker, New York, 1976), p. 88.
15. F.G. Bonica, N. Spataru and T. Spataru, *Electroanalysis* **9** (1997) 1341.
16. A.R. Despic and V.D. Jovic, *in* R.E. White, J.O.M. Bockris and B.E. Conway (Eds), 'Modern Aspects of Electrochemistry', Vol. 27 (Plenum Press, New York, 1995), p. 143.